Received: 1 June 2021 | Accepted: 29 July 2021

DOI: 10.1002/2050-7038.13068

RESEARCH ARTICLE

WILEY

# Sequential model predictive control of quasi Z-source inverter with fixed frequency operation

**Siva Kumar Gannamraju** | **Ravikumar Bhimasingu**

Department of Electrical Engineering, Indian Institute of Technology, Hyderabad, Telangana, India

**Correspondence**
Ravikumar Bhimasingu, C-409, Academic Block-C, Department of Electrical Engineering, Indian Institute of Technology, Hyderabad, Kandi, Sangareddy, Telangana 502285, India.
Email: ravikumar@ee.iith.ac.in

**Summary**

Quasi Z-source inverter (qZSI) is a single-stage high gain buck-boost converter suitable for various applications like renewable energy sources, power electronic drives, and power supply systems. Controller design for qZSI should ensure simultaneous control of multiple objectives such as the DC capacitor voltage, source inductor current, and load current. While controllers dealing with multiple objectives, obtaining a good steady-state and transient performance with low control complexity is essential. Fortunately, Model Predictive Control (MPC) is emerging as an effective alternative that can address all the above-said issues simultaneously. However, some of the severe problems to be addressed with the conventional MPC algorithms developed for qZSI are applying a single vector per sampling duration, higher computational requirements, and lack of analytic procedure to handle weight factors. This paper presents a control algorithm with features of weight factor elimination and AC load current ripple reduction by using a modified double vector predictive control approach with fewer computational requirements. The principle of inclusion of zero vector, weight factor elimination, and a detailed calculation for duty ratio are included. As the converter operates at a fixed frequency, significant ripple reduction for DC current, link voltage, and load current ripple have been achieved. The proposed MPC requires only $\approx 81\%$ of computations needed for the conventional MPC. Methodological comparison has been provided to present the superiority of the proposed MPC compared to appropriate conventional MPCs available in the literature.

**KEYWORDS**

duty ratio optimization, model predictive control, quasi Z-source inverter, weight factors

**List of Symbols and Abbreviations:** ($S_1$-$S_6$), inverter switches; $L_f$, load side inductor; $R_f$, internal resistance of the load side inductor; $L_1$, $L_2$, input inductances; $C_1$, $C_2$, input capacitances; $R$, load resistance; $i_o$, per phase load current; $v_o$, per phase load voltage; $I_{L1}$, $i_{L2}$, DC inductor current; $V_{C1}$, $V_{C2}$, DC capacitor voltage; $V_{DC}$, DC supply voltage; $i_{inv}$, inverter input current; $T_s$, sampling period; $\lambda$, weight factors; $D$, DC side duty ratio; $V_{link}$, DC link voltage; $i_{ref}$, load current reference; $f_s$, AC frequency; $p_{loss}$, total loss of an IGBT; $p_{sw}$, switching loss of an IGBT; $k$, proportional constant; $p_{loss,cond,ST}$, conduction loss of an IGBT during shoot-through state; $p_{loss,cond,nST}$, conduction loss of an IGBT during non-shoot-through state; $I_{a,error}$, phase 'a' load current error; AC, alternating current; ADC, analog to digital conversion; CSI, current source inverter; DC, direct current; DSP, digital signal processor; EMI, electromagnetic interference; FPGA, field programmable gate array; IDE, integrated development environment; IGBT, insulated gate bipolar transistor; ISR, interrupt service routine; MPC, model predictive control; MPPT, maximum power point tracking; OSV-MPC, optimal switching vector MPC; PI, proportional integral; PLL, phase locked loop; PSO, particle swarm optimization; qZSI, quasi Z-source inverter; RMS, root mean square error; SPWM, sinusoidal pulse width modulation; SVPWM, space vector pulse width modulation; THD, total harmonic distortion; VSI, voltage source inverter.

  

## 1 | INTRODUCTION

Generally, it is a two-stage system to transform a low voltage DC to a high voltage AC, as the conventional two-level three-phase Voltage Source Inverter (VSI) is a buck converter. Although such an operation may create an additional DC port, it results in lower system efficiency, requires more hardware and extra switch count compared to the single-stage converter.[1,2]

Z-source inverter (ZSI) was developed as a single-stage converter to improve dead-band elimination, EMI issue handling facility, buck-boost operation, and be managed as a VSI or CSI.[3] In Anderson et al,[4] an improved version of ZSI, named quasi-ZSI (qZSI) was developed to get the extra facilities of continuous supply current, common ground connecting DC link and DC supply, and a small passive component. Later, many reshape were developed for qZSI, but each adaption has its issues and complications.[5] qZSI has been tested to many applications such as solar PV systems,[6] adjustable speed control drives,[7,8] microgrid applications,[9] multi-port converter for battery applications,[10] and electric vehicle applications in Battiston et al.[11,12] In Guo e al,[13] a high performance 85 kW inverter was developed and tested under various conditions to test the suitability of qZSI for electric vehicle applications.

However, the controller design of qZSI is a challenging task as it is required to control the DC capacitor voltage, DC source current and load current (in the case of motor control and grid applications) simultaneously. Usually, DC side modulation is performed by simple boost, maximum boost, constant boost, and AC side modulation is performed with the SPWM and SVPWM modulation.[14-16] Along with these modulation schemes, PI-based control implementation is a general practice. However, the conventional industrially accepted PI control suffers from rise time and bandwidth issues in applications where superior dynamic performance is obligatory such as distributed generations, grid-connected systems, and renewable interfacing.[17] In addition, the situation becomes complex if the converter is managed as a multi-port system, as the tuned parameters may not give decent performance over a wide range of operating circumstances.

The above-considered issues drive the researchers to look toward alternative algorithms, exclusively the sample-based algorithms that need to be executed on a high-level computational platform. Over the last decade, due to the advent of high-speed DSPs, microprocessors, and FPGAs researchers focused on sample-based advanced control techniques such as sliding mode control, intelligent control systems, model predictive control, and so on..[17] MPC has gained much attention among researchers due to its remarkable features such as multi-objective handling, multi constrain handling, intuitiveness, and superior dynamic performance.[18,19] MPC (OSV-MPC) is a model-based optimization approach that minimizes the cost function to select an optimal switching vector for every sampling duration.[20,21] However, the basic OSV-MPC[22,23] applies a single vector in each sampling duration[24,25] which in turn produces poor THD performance, EMI issues, ripples in the control variables, and difficulties in the filter design.[26,27] In addition, due to the higher computational requirements and the disadvantages of variable switching frequency, in many applications, the steady-state performance of the conventional single vector MPC is poor.[28] To counter these issues, various predictive control algorithms were investigated based on the application of double vectors or multiple vectors for some applications in each switching duration.[27,29] Multi-vector based predictive control methods generally require more processing power.[30] A pre-defined switching sequence-based fixed frequency predictive control which applies three vectors in a sampling duration (two active vectors and a zero vector) discussed in Tarisciotti et al[27] requires complex cost functional formulations. Another drawback of multi-vector based predictive controls is their higher computational demand.[28] While controlling a multi-port converter, other requirements such as protection supervision and other auxiliary tasks (such as ADC measurements, MPPT for renewable applications, synchronization for grid-connected applications) also require significant computational powers. To reduce the computational powers and switching operations without sacrificing the load current ripple, double vector approaches provide optimal performance.[31]

A basic MPC algorithm for qZSI was established in Ellabban et al.[32,33] A comparison was made with the PI controller based method[34] and presented the advantages of MPC in terms of steady-state ripple, control complexity, and transient performance. However, the problem with the basic MPC approach[33] is that the weight factors have to be dynamically changed to achieve high performance when the control variable reference values change.[35] Though other methods such as fuzzy logic,[36] genetic algorithms,[37] and neural networks[38] may be used to tune the weight factors, they are computationally inefficient and require offline adjustment. Moreover, application of these methods to tune the weight factors loses the intuitiveness of the basic MPC. In Bakeer et al,[39] an algorithm was proposed to reduce the number of sensors by extrapolating the inductor current. Another algorithm was proposed in Bakeer et al[40] to reduce the computations but it suffers from high ripple at the AC side current due to the application of the single vector in a sampling duration. An algorithm was recently developed[41] using logical operations to eliminate the weight factors, but the concept of

shoot-through remains the same as.[40] Moreover, this algorithm utilizes only a single vector, and the results show many ripples in the AC side current. As the switching frequency is not fixed, the filter design also becomes an arduous task.

Double vector-based predictive control of qZSI was proposed in Liu et al[42,43] requires weight factor tuning, uses the same concept of shoot-through-based separation of inductor current as[40] to simplify the basic MPC algorithm. To solve the problem of weight factors, sequential predictive control[44] has been recently proposed. In Norambuena et al[44] the optimal vectors are selected based on the cascaded optimization which includes many control objectives in the cost function. Later modified versions of the sequential predictive control for induction motor control[44,45] mentioned the importance of selecting the optimum number of vectors for satisfactory operation without losing the priority for the control variables.

Based on the above description, it can be observed that there is a need to solve the problems of weight factor tuning and achieve high performance at both AC and DC sides simultaneously. So, this paper presents a double vector-based sequential predictive control method that provides duty ratio operation for the shoot-through as well as non-shoot-through operation. Any of the conventional shoot-through techniques such as simple boost, maximum boost, or constant boost can be included with the proposed method.[15] The optimal vectors are chosen based on the cascaded optimization, which includes multiple control objectives in the cost function. The optimal vectors are identified based on the cascaded optimization, which includes multiple control objectives in the cost function. In addition, the performance is compared with the weight factor-based algorithm,[33] and detailed performance analysis is presented under various operating conditions. The contributions of this paper are as follows,

- Provides fixed switching frequency based algorithm operation so that the steady-state ripple gets reduced.
- Presents weight factor less algorithm for the control of qZSI.
- Analysis and verification of the proposed algorithm under various operating conditions.

Organization of the paper is as follows. Section 2 exhibits the mathematical model of qZSI. Section 3 describes the conventional model predictive control for qZSI. Section 4 discusses the proposed model predictive control for qZSI. Section 5 provides the simulation results and experimental validation under various operating conditions. Section 6 concludes the proposed work.

## 2 | MATHEMATICAL MODEL OF THE QZSI

This section describes the basic mathematical model of the qZSI[34] shown in Figure 1A. The Z source network at the DC side acts as the boost circuit and maintains symmetrical operation. The inverter switches ($S_1$-$S_6$) acts as the control circuit for the energy conversion from the DC side to the AC side. Load side inductor $L_f$ represents the AC side filter to eliminate the high-frequency components, and $R_f$ represents the internal resistance of the load side inductor $(L_f)$. Resistance ($R$) acts as the load and is the same throughout the operation. $i_{o,a}, i_{o,b}$ and $i_{o,c}$ represent the load phase currents. $v_o$ represents the per-phase load voltage on the AC side. $V_{\mathrm{DC}}$ represents the supply side voltage and $i_{L_1}$ is the supply current. The basic qZS network contains two inductors, two capacitors, and a diode, as shown in Figure 1A. $V_{C_1}$ and $V_{C_2}$ represent the voltages of the two capacitors whose capacitance are $C_1$ and $C_2$ respectively, and $i_{L_1}$ and $i_{L_2}$ represents the currents of the two inductor's whose inductance are $L_1$ and $L_2$, respectively. Diode $D_1$ helps to maintain the proper energy transfer to the load during non-shoot-through state. $i_{\mathrm{inv}}$ is the inverter input current. Based on the switch positions, there are six active vectors $(V_1, V_2, V_3, V_4, V_5, V_6)$, two zero vectors $(V_8, V_7)$, and a shoot-through state $(V_9)$ which are described in Figure 4 in the $\alpha\beta$ plane of qZSI vector diagram. It should be noted that for the conventional two-level three-phase VSI, no two switches in the same leg should be turned on simultaneously, but the qZSI has another state, namely shoot-through state $V_9$ in which both the switches in the same leg are turned on simultaneously.

Circuit diagrams describing the shoot-through and non-shoot-through states are shown in Figure 1B and Figure 1C, respectively. During the shoot-through state, the two inductors charge, and during the non-shoot-through state, the stored energy in the inductors gets discharged to the load. Supply side inductor's resistance and equivalent static resistance (ESR) of the capacitors are negligible to simplify the mathematical model.

To obtain the symmetry, it is assumed that the two inductors $(L_1, L_2)$ are identical and two capacitors $(C_1, C_2)$ are identical. Then their respective voltages and currents can be represented by (1) and (2).

$$V_{C_1} = V_{C_2} = V_C \tag{1}$$

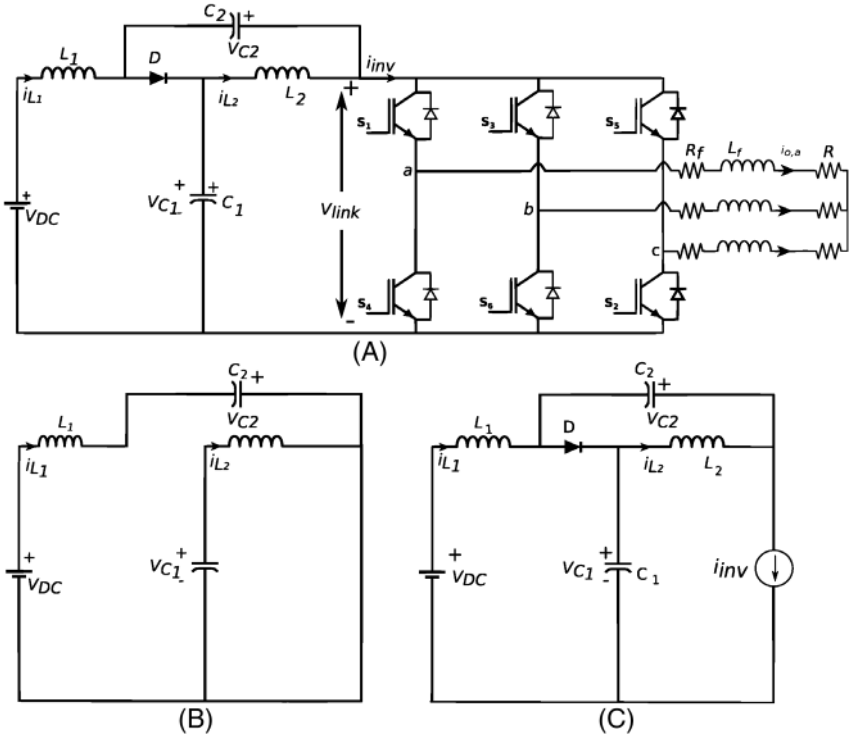


**FIGURE 1** A, Circuit diagram of quasi Z-source inverter, B, Shoot-through operation, C, Non-shoot-through operation

$$i_{L_1} = i_{L_2} = I_L \tag{2}$$

During the shoot-through (as shown in Figure 1B) condition, by applying Kirchhoff laws, the mathematical model can be expressed as (3) and (4).

$$L_1 \frac{di_{L_1}}{dt} = V_{\mathrm{DC}} + V_{C_2} \tag{3}$$

$$C_1 \frac{dV_{C_1}}{dt} = -i_{L_2} \tag{4}$$

During the non-shoot-through state (as shown in Figure 1C), the mathematical model can be expressed as (5) and (6).

$$L_1 \frac{di_{L_1}}{dt} = V_{\mathrm{DC}} - V_{C_1} \tag{5}$$

$$C_1 \frac{dV_{C_1}}{dt} = i_{L_1} - i_{\mathrm{inv}} \tag{6}$$

Applying Kirchhoff laws at the AC side as shown in Figure 1A, provides the relation between load voltage, load current, and the filter parameters which can be expressed as (7).

$$v_{o,a} = L_f \frac{di_{o,a}}{dt} + \left(R + R_f\right) i_{o,a} \tag{7}$$

To control the inductor current, the state space representation of the inductor current can be derived from (7) as (8).

$$L_f \frac{di_{o,a}}{dt} = v_{o,a} - \left(R + R_f\right) i_{o,a} \tag{8}$$

## 3 | CONVENTIONAL MODEL PREDICTIVE CONTROL OF QZSI

The basic MPC algorithm requires the mathematical model of the system, which is described in Section 2. Once the system model is obtained, the future values of the sensed parameters have to be calculated using numerical differentiation methods such as the Euler method.[17] To obtain the discrete model, Euler's first order formula has been used to calculate the one step ahead prediction of the inductor current $(i_{L_1})$ and capacitor voltage $(V_{C_1})$ by using the mathematical model described in Section 1. During shoot-through state, inductor current, and capacitor voltage at the $(k+1)$ instant are obtained as (9) and (10), respectively.

$$i_{L_1}(k+1) = \frac{L_1 i_{L_1}(k) + T_s(V_{C_1}(k))}{L_1} \tag{9}$$

$$V_{C_1}(k+1) = V_{C_1}(k) - \frac{T_s}{C_1} i_{L_1}(k+1) \tag{10}$$

where $T_s$ is the sampling duration. During the non-shoot-through (active) states, the voltage, and current predictions at $(k+1)$ instant are (11) and (12), respectively.

$$i_{L_1}(k+1) = \frac{L_1 i_{L_1}(k) + T_s(V_{\mathrm{DC}} - V_{C_1}(k))}{L_1} \tag{11}$$

$$V_{C_1}(k+1) = V_{C_1}(k) + \frac{T_s}{C_1}(i_{L_1}(k+1) - i_{\mathrm{inv}}(k+1)) \tag{12}$$

During the non-shoot-through (zero) states, the capacitor voltage, and inductor current are expressed as (13) and (14), respectively.

$$i_{L_1}(k+1) = \frac{L_1 i_{L_1}(k) + T_s(V_{\mathrm{DC}} - V_{C_1}(k))}{L_1} \tag{13}$$

$$V_{C_1}(k+1) = V_{C_1}(k) + \frac{T_s}{C_1} i_{L_1}(k+1) \tag{14}$$

Equations (9) to (14) can be calculated at $(k+2)$ instance to avoid the computational delay involved in the algorithm implementation during the experimental operation. To avoid an additional sensor requirement, the inverter input current $(i_{\mathrm{inv}})$ mentioned in (12) has been estimated using the switch conditions and load currents as per the Equation (15).

$$i_{\mathrm{inv}} = S_a i_{o,a} + S_b i_{o,b} + S_c i_{o,c} \tag{15}$$

At the load side, three currents are measured to identify the future one step ahead prediction of load currents. Measured values of $(i_a, i_b, i_c)$ are converted to $(i_\alpha, i_\beta)$ to reduce the computations. The one step ahead load current can be calculated as,

$$i_{o,\alpha}(k+1) = \left(1 - (R+R_f)\frac{T_s}{L}\right) i_{o,\alpha}(k) + \frac{Ts}{L}(v_o) \tag{16}$$

where $v_o$ is expressed as,

$$v_o = \frac{2}{3} V_{\mathrm{DC}}(S_1 + aS_2 + a^2 S_3) \tag{17}$$

where $S_1, S_2, S_3$ are the switching states for the upper switches in each leg of the three phase inverter. To compensate the delay involved in the control algorithm, two step ahead prediction can be calculated as (18).

$$i_{o,\alpha}(k+2)=\left(1-\left(R+R_f\right)\frac{T_s}{L_1}\right)i_{o,\alpha}(k+1)+\frac{Ts}{L_1}(v_o(k)) \tag{18}$$

As per the principle of OSV-MPC, the actual values should track the future references at $(k+1)$ or $(k+2)$ instance based on the extrapolation. Though the THD performance is unaffected, significant steady-state error results from the lack of extrapolation. Third-order two-step ahead reference equation is used to estimate $i_{o,\alpha,\mathrm{ref}}$[17] as,

$$\begin{aligned} i_{o,\alpha,\mathrm{ref}}(k+2)=10i_{o,\alpha,\mathrm{ref}}(k)-20i_{o,\alpha,\mathrm{ref}}(k-1)\\ +15i_{o,\alpha,\mathrm{ref}}(k-2)-4i_{o,\alpha,\mathrm{ref}}((k-3) \end{aligned} \tag{19}$$

Similarly, extrapolation has been performed for $i_{o,\beta,\mathrm{ref}}$.

As per the basic MPC algorithm,[33] the cost function is the absolute difference of the predicted control variable (one step ahead prediction) and the extrapolated reference value. To calculate the extrapolated reference, Lagrange extrapolation is used for every sampling period as depicted in (19), the predicted values are calculated for each and every switching state, including shoot-through and non-shoot-through so that the cost function also gets calculated for every switching state. The final cost function is the sum of individual cost functions. The final cost function and individual cost functions of the supply current, DC capacitor voltage, and load current are shown in (20).

$$\begin{aligned} g_1 &= |\, I_{L,\mathrm{ref}}^{k+2}-I_{L_1}^{k+2}\,|\\ g_2 &= |\, V_{C,\mathrm{ref}}^{k+2}-V_{C_1}^{k+2}\,|\\ g_3 &= |\, i_{o,\alpha,\mathrm{ref}}^{k+2}-i_{o,\alpha}^{k+2}\,|+|\, i_{o,\beta,\mathrm{ref}}^{k+2}-i_{o,\beta}^{k+2}\,|\\ g &= \lambda_1 g_1+\lambda_2 g_2+\lambda_3 g_3 \end{aligned} \tag{20}$$

where the values of $\lambda_1$, $\lambda_2$, $\lambda_3$ are called as weight factors and are estimated based on the heuristic approach. Similarly, the value of $i_{o,\beta}(k+2)$ has to be calculated (similar to (18)) to find the cost function.

The weight factors represent the relative importance and priority of the control parameters. So it should also be observed that these weight factors are not unique for a particular operating condition.[46] Whichever switching state results in minimizing the cost function, that is, produces the least error ($g$), that particular state gets applied to the inverter.

## 4 | PROPOSED WEIGHT FACTOR LESS FIXED FREQUENCY BASED PREDICTIVE CONTROL FOR QZSI

Figure 2 shows the control block diagram of the proposed algorithm and the algorithmic differences concerning the conventional MPC can be obtained from the same. The proposed method is similar to the conventional way of delaying compensation for the sensed parameters and extrapolating the reference parameters. The shoot-through-duty ratio is calculated separately for the DC side based on the inductor current to eliminate the weight factors. In the conventional MPC, the same inductor current error has to be calculated for the non-shoot-through states to identify the best optimal vector. Every time, all the capacitor voltage errors have to be identified for optimal operation. Only the best three vectors obtained from the load current have to be optimized. This simplifies the algorithm and reduces the computations significantly.

Tuning the weight factors over a range of operating conditions is a tedious task, and improper tuning of the weight factors causes the system to be unstable. This work eliminates the weight factors and includes a cascaded optimization. Simultaneously, to make the filter design easy and improve the steady-state ripple, this work provides a fixed frequency operation by employing duty ratio operation at the AC and the DC side. The proposed method is described in three sections: DC side duty ratio calculation, sequential optimization, and AC side duty ratio calculation. Compared to the conventional predictive control (shown in Figure 2), the proposed predictive control arranges separate cost functions for each control objective, namely load current ($i_o$), DC capacitor voltage ($V_{C_1}$), and inductor current ($i_{L_1}$).

### 4.1 | DC side duty ratio calculation

As per the system model of qZSI, the DC side inductor current is different for shoot-through and non-shoot-through states, whereas the capacitor voltage is different in all the three states, namely active states, zero, and shoot-through

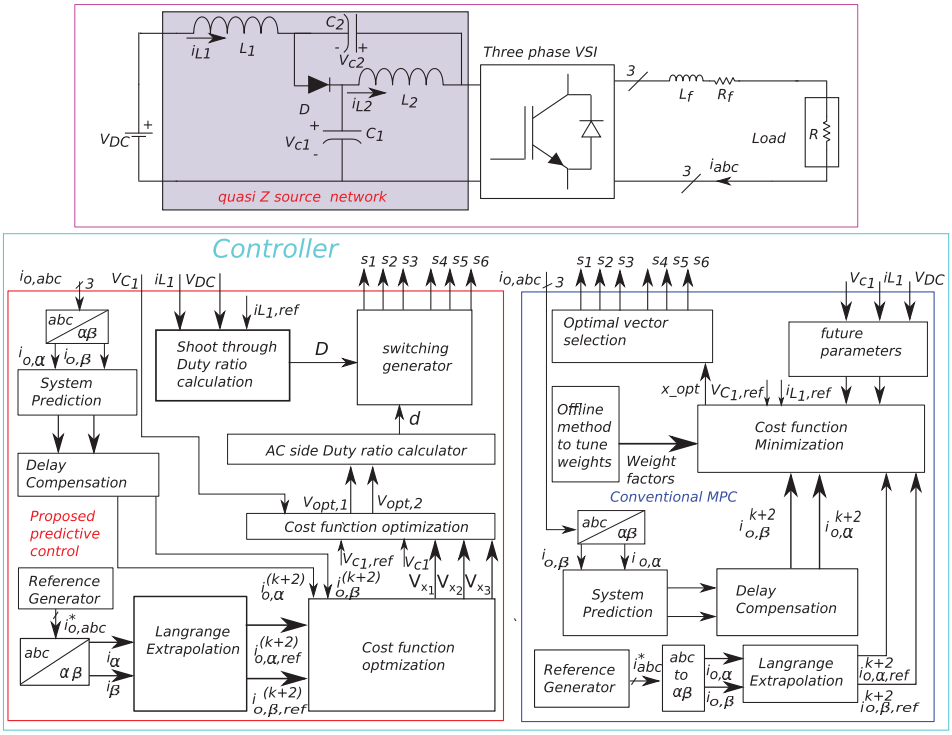


FIGURE 2 Control block diagram of quasi ZSI with the conventional predictive control and the proposed predictive control

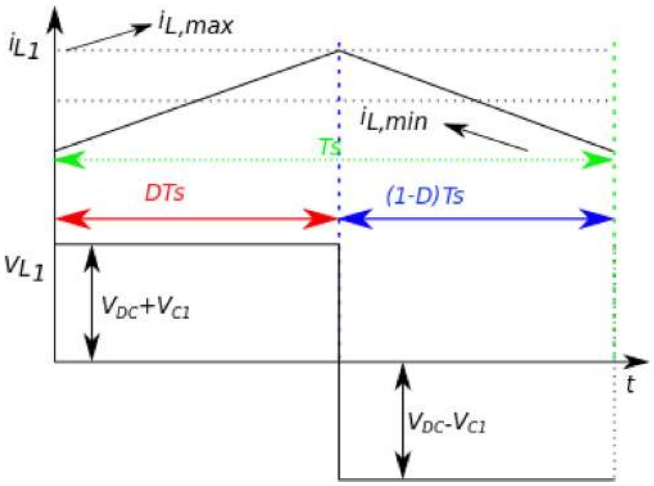


FIGURE 3 Shoot-through duty ratio description

form. This feature has been utilized in the proposed controller to felicitate the weight factor less algorithm. Based on the inductor current error minimization, the shoot-through state or non-shoot-through state is to be applied. Supply-side inductor current during shoot-through and non-shoot-through states are described in (9) and (11), respectively. To calculate the shoot-through duty ratio, the principle of volt-sec balance has been applied. From Figure 3, it can be seen that the steady-state inductor current constantly oscillates between the $i_{L,\max}$ and $i_{L,\min}$. It can be observed that during shoot-through state, the inductor charges, and during the non-shoot-through state, the inductor discharges. From Figure 3 and Equations (9) and (11), the average inductor current can be expressed as (21).

$$i_{L_1}(k+1) = i_{L_1}(k) + \frac{T_s((1-D)(V_{\mathrm{DC}} - V_C) + DV_C)}{L_1} \tag{21}$$

To minimize the load current error, the condition $i_L(k+1) = i_{L,\text{ref}}$ has to be satisfied. Further simplification provides the expression for duty ratio as described in (22).

$$D = \frac{\frac{T_s}{L_1}(i_{L_1,\text{ref}}) - i_{L_1}(k+1) - V_{\text{DC}} + V_C}{2V_C - V_{\text{DC}}} \tag{22}$$

Similarly, this duty ratio calculation can be extended to any number of samples ahead prediction such as $i_{L_1}(k+2), i_{L_1}(k+3)$. Here $i_{L_1,\text{ref}}$ can be calculated using the power balance relating the reference power and supply voltage. While providing the one step ahead duty ratio, the capacitor voltage is neglected during the shoot-through operation.[40] However, the inclusion of shoot-through capacitor voltage can also be done by writing the relationship between one step ahead capacitor voltage and one step forward inductor current.

## 4.2 | Sequential optimization

To eliminate the capacitor voltage weight factor that's present at the AC side (as mentioned in (20)), a cascaded optimization[44] has been adopted in this work. Two control variables, namely load current and DC Capacitor voltage, must be optimized to identify the best optimal vector. The two cost functions at the AC side are load current ($i_o$) error minimization (23) and the capacitor voltage ($V_C$) error minimization (24).

$$g_1 = | i_{o,\alpha,\text{ref}}^{k+2} - i_{o,\alpha}^{k+2} | + | i_{o,\beta,\text{ref}}^{k+2} - i_{o,\beta}^{k+2} | \tag{23}$$

$$g_2 = | V_{C,\text{ref}}^{k+2} - V_C^{k+2} | \tag{24}$$

It is to be observed that there are seven different switching instances ($V_1$ to $V_7$), out of which the best switching vector optimizes the load current error and the capacitor voltage error. In special cases such as thermal performance improvement and switching frequency reduction, there is a chance of considering both the zero states in the optimization. In the proposed algorithm, all the six active states ($V_1$ to $V_6$) and two zero states ($V_7, V_8$) are involved in the optimization process to have more flexibility to apply $V_7\,(1,1,1)$ or $V_8\,(0,0,0)$ as a zero vector. During the proposed optimization process for qZSI, the two control parameters, namely the load current error and capacitor voltage error, have to be optimized. Especially when the port at capacitor is operated with loads, this becomes an issue. However, for the basic boosting operation, the "load current should be given priority as there is an inherent dependency of the DC capacitor voltage on the load current (can be observed from (12) and (15)) so that the computational burden, as well as the steady-state load current ripple, can be reduced significantly."

Initially, all the possible errors, namely $g_1^1$ to $g_1^8$ have been identified for the load current. After identifying the errors, arrange them in an ascending order to find the associated optimal vectors. Of all the errors, find out the three best possible vectors with a minimum error that gives optimum performance. Even four best vectors or higher can be selected, but it is always a trade-off between the computational requirements and the optimal performance for the load current. Considering more vectors reduces the importance of the load current. But to perform the sequential optimization, at least two vectors are required to control the capacitor voltage.[24,44] Here to improve the ripple performance, the three best vectors are considered. The vector with minimum capacitor error has to be selected. After selecting the best vector for an optimal duty ratio operation (which is described in the latter part of Section 4.2), the second vector can be zero vector to get the constant switching frequency operation.[29] This principle of a combination of an active vector and a zero vector can be explained in Figure 4. Let us consider that in a sampling duration, if active vector alone is applied, then the particular error (absolute difference between the reference and an actual value) is " $e_1$," and if a combination of active and zero vector is applied, then the corresponding error is " $e_{01}$." So from Figure 4, the errors for both the methods are related as $\{e_{01} < e_1\}$. Here the reference vector $V_{\text{ref}}$ is represented in blue color. The error reduction can easily be observed from Figure 4 concerning the color-coding. The error (which is perpendicular to the $V_4$) represented with green color is based on the proposed method, and the error vector represented with red color is based on the conventional MPC. Similarly, the same concept can be observed with vector $V_6$, $e_2$ (represented in pink), and $e_{02}$ (represented in black). When applying $V_6$, the error $\{e_2 > e_{02}\}$. Where $e_2$ is the error due to the application applying the vector

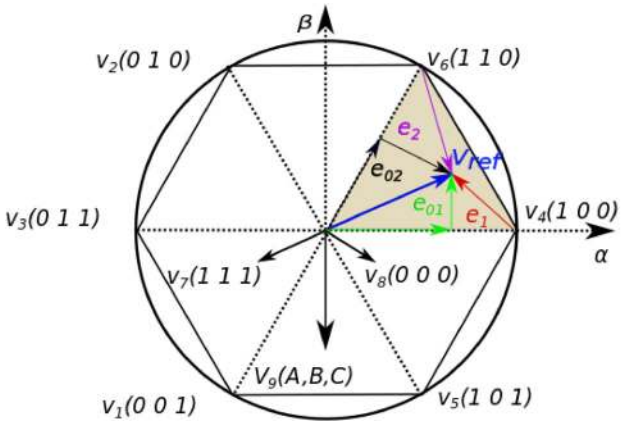


**FIGURE 4** qZS inverter space vector diagram

$V_6$ for the complete $T_s$ duration and $e_{02}$ is the error due to the application of a combination of an active vector $V_6$ and a zero vector ($V_7$ or $V_8$) in the $T_s$ duration. This is similarly the case with any of the sectors in the space vector diagram. After identifying the best vector, the combination with a zero vector can be applied in every sampling duration. The selection of the zero vector out of two available states ($V_7$ (0,0,0) or $V_8$ (1,1,1)), is based on the switching minimization. For the vectors, $V_1$ (0,0,1), $V_2$ (0,1,0), $V_4$ (1,0,0), the vector $V_7$ (0,0,0) is identified as zero vector and for the remaining vectors $V_3$ (0,1,1), $V_5$ (1,0,1), $V_6$ (1,1,0), the vector $V_8$ (1,1,1) is identified as the zero vector. Here, the load current performance and capacitor voltage highly depend on the selection of the number of optimal vectors from the cost function. The reason for selecting the three best vectors instead of one vector is to provide the improved steady-state performance of the capacitor voltage.[45]

## 4.3 | AC side duty ratio calculation

Once the two vectors are identified, their respective duty ratios have to be calculated. The resultant vector is calculated from its relation with the duty ratio, and the selected optimal vectors are as per (25).

$$V_{\text{res}} = V_{\text{opt},1} d + (1-d) V_{\text{opt},2} \tag{25}$$

where "$d$" is the duty ratio and $V_{\text{opt},1}$, $V_{\text{opt},2}$ are the best selected vectors obtained from sequential optimization (Section 4.2). It is to be understood that the first vector can be an active vector or a zero vector. If the optimal vector selected is an active vector, the procedure for selecting the zero vector is described in Section 4.2. However, if the vector is a zero vector, the second vector is also a zero vector.

It is to be understood that for the entire duration, the zero vector has to be applied. However, the selection of the zero vector should not get conflicted with the shoot-through operation. So to get the implementation of the shoot though process, if the first vector is a zero vector, then the zero vector selected should be $V_8$(1,1,1). At the DC side, the shoot-through state can be operated sequentially for three inverter legs. That is, implementation of shoot-through operation for one leg in a sampling interval. Once the vector $V_{\text{opt1}}$ is selected based on the basic principle of predictive control as in Kouro et al,[20] the duty ratio calculation involving the load current minimization can be explained as (26).

$$\begin{aligned} i_{o,\alpha,V_{\text{opt1}}}(k+2) = \Bigg\{ & \left(1 - \left(R + R_f\right)\frac{T_s}{L}\right) i_{o,\alpha}(k+1) \\ & + \frac{Ts}{L_f}\left(d^{*} v_{o,V_{\text{opt1}}}(k+1)\right) \Bigg\} \end{aligned} \tag{26}$$

If the optimal vector is a zero vector ($V_7$ or $V_8$), then the relation between the future load current and the selected vector can be represented as,

$$i_{o,\alpha,z}(k+2)=\left(1-\left(R+R_f\right)\frac{T_s}{L_f}\right)i_{o,\alpha}(k+1) \tag{27}$$

Then the corresponding error for the optimal vector can be calculated as (28).

$$g_{i,V_{\text{opt1}}}=\left|i_{\text{ref}}-i_{o,\alpha,V_{\text{opt1}}}\right|^2 \tag{28}$$

Based on the Deadbeat control principle, an optimization of $g_{i,V_{\text{opt1}}}$ with respect to " $d$" is performed as shown in (29).

$$\frac{\partial g_{i,V_{\text{opt1}}}}{\partial d}=0 \tag{29}$$

Finally " $d$" is obtained from (30).

$$d=\left\{\frac{i_{o,\alpha,\text{ref}}-i_{o,\alpha z}}{\left(\frac{T_s*\left|v_{o,V_{\text{opt1}}}(k+1)\right|^2}{L_f}\right)}\right\}*v_{o,V_{\text{opt1}}}(k+1) \tag{30}$$

where $i_{o,z,\alpha}$ is the value of load current when a zero voltage vector is applied.

The detailed flowchart describing both methods is provided in Figure 5. From the flow chart, it is clear that, with the proposed algorithm, "all the inductor currents errors and all the capacitor voltages errors need not be calculated for every for loop," so as a result, there will be a significant reduction of computations. Although there are some extra calculations for the duty ratio, still the computation requirements are more for conventional MPC. Details on the computational requirements for the proposed algorithm are discussed in Section 5.

## 5 | SIMULATION AND EXPERIMENTAL RESULTS

### 5.1 | Simulation results

To identify the proposed algorithm's improvements, simulations have been performed and compared with the conventional weight factors-based method.[33] Both the methods are verified under the same operating conditions, and simulation parameters are mentioned in Table 1. In the case of conventional MPC, the switching frequency is variable. The same switching frequency is considered for both the conventional and proposed methods to provide a clear comparison. Figures 6 and 7 show the simulation results with the conventional predictive control and the proposed predictive control, respectively, for a step-change in load. But compared to the conventional MPC, the proposed control ripple is less than 2.5%. At the DC side, with the conventional weight factor-based predictive control, before the application of step change, the inductor current ripple is 3 A whereas, the proposed control has produced only a ripple of 2.5 A. The improvement in the ripple performance is due to the presence of the fixed frequency operation and weight factor tuning in the case of conventional MPC. The DC link voltage ($V_{\text{link}}$) is observed to be tracking the steady-state with a ripple of less than 2% even after the step change of load at the time of 2 seconds as shown in Figures 6 and 7. Zero link voltage ($V_{\text{link}}$) for each case can be identified for both figures during the shoot-through and non-shoot-through operations. For the step change in load power, the current reference from 2 to 3 A is performed at time 2 seconds. Both the methods settled to the provided reference value without any peak overshoots and settled in few samples. Observing these results, the proposed method has superior performance in terms of AC current ripple and reduced ripple at the DC side current.

Figures 8 and 9 represented the Total Harmonic Distortion (THD) plots for conventional MPC and proposed MPC, respectively. It can be observed that the spectrum of the MPC has spread over a spectrum (up to 20th harmonic considered) whereas in the proposed controller, only the 5th, 7th, 11th, 13th, 17th harmonics are superior, which indicates

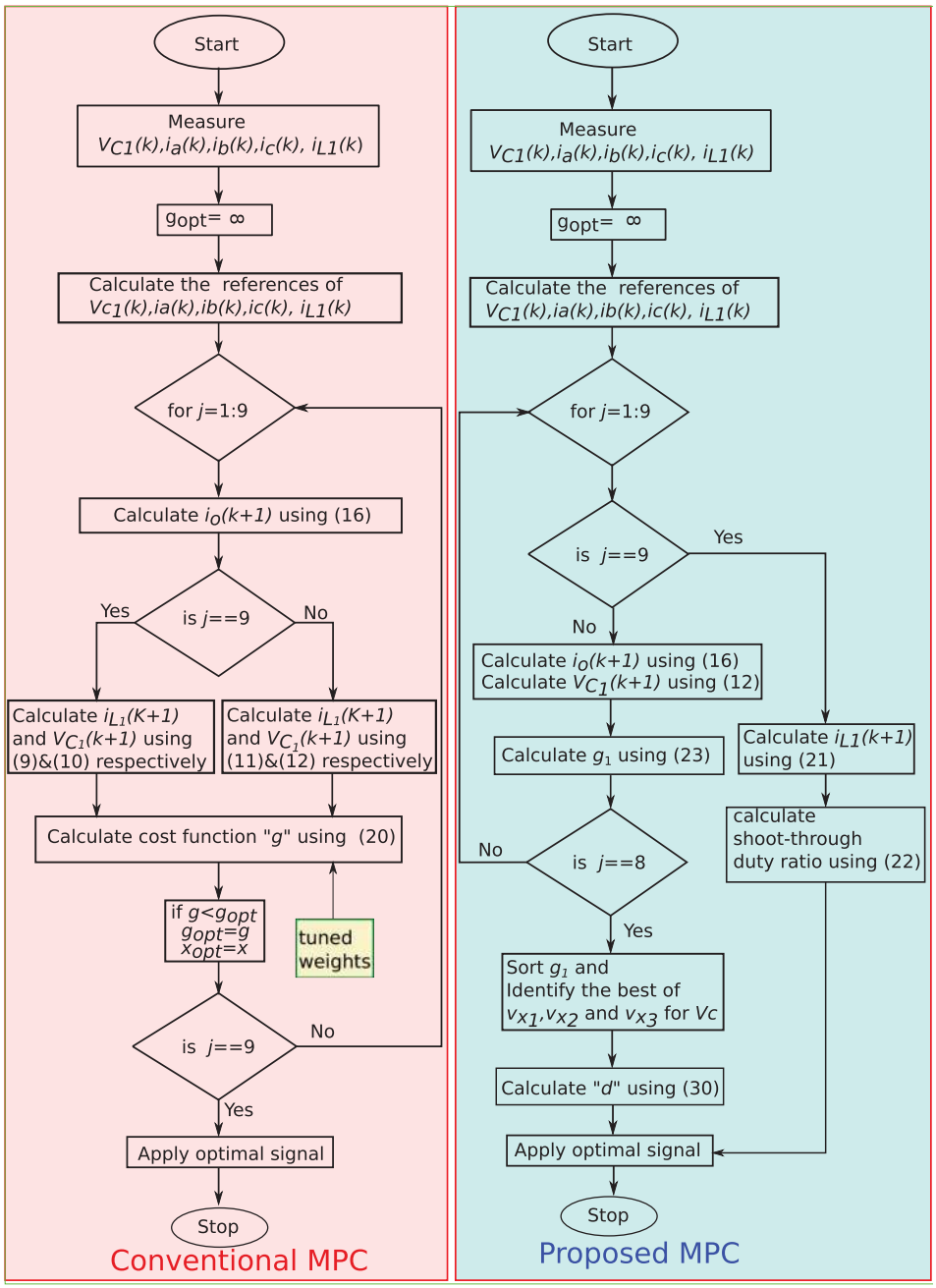


**FIGURE 5** Flow chart describing the procedural differences between the conventional predictive control and the proposed predictive control at one step prediction

**TABLE 1** Simulation parameters

| Parameter | $V_{DC}(V)$ | $V_{C,ref}(V)$ | $L_1(H)$ | $L_f(H)$ | $C_1(F)$ | $R\ (\Omega)$ | $R_f\ (\Omega)$ | Fsw (KHz) | $F_s$(KHz) |
|---|---|---|---|---|---|---|---|---|---|
| Value | 50 | 110 | 1 | 10 | 470 | 10 | 0.2 | 8 | 25 |

that the proposed method obtained the characteristics of the duty ratio operation. At the same time with the proposed method, the THD of the proposed method is 2.46%, whereas, with the conventional MPC, it is 4.25%. This clearly shows that the application of duty ratio for the predictive controller reduced the steady-state ripple and reduced the load current THD.

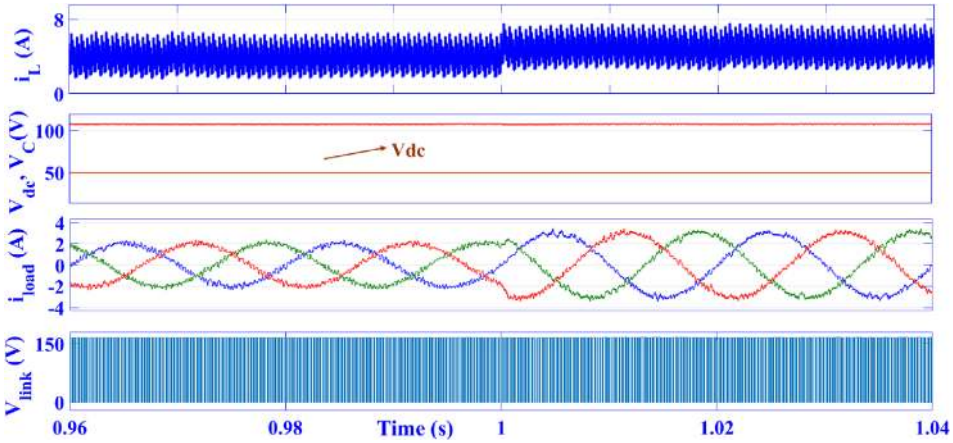


FIGURE 6 Results of the conventional MPC for a step change in load power

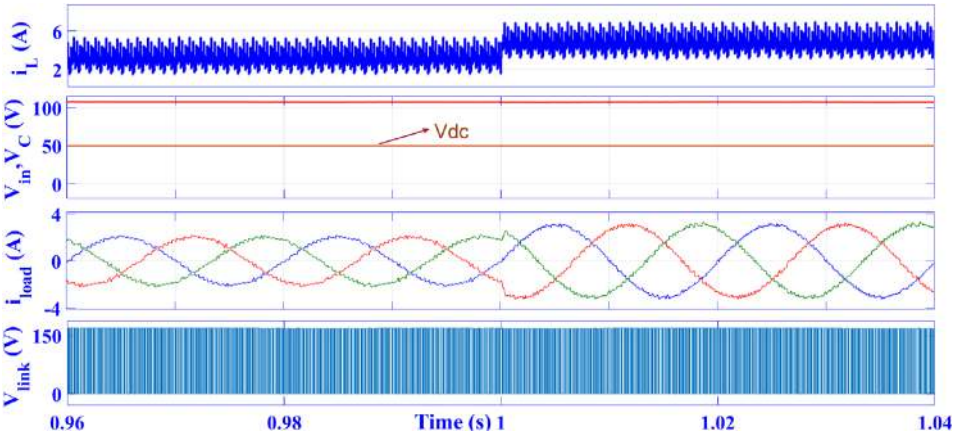


FIGURE 7 Results of the proposed MPC for step change in load power

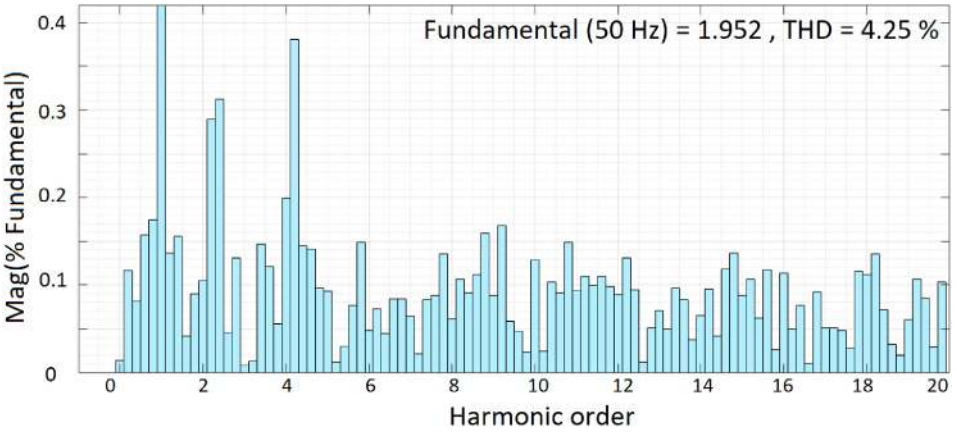


FIGURE 8 THD plot of the load current for the conventional MPC

## 5.2 | Experimental results

For control algorithm implementation, a dual-core processor, TMS320F28377s, has been used. Code Composer Studios is the IDE (integrated development environment) platform for algorithmic implementation. The number of calculations has been presented for each control method in Table 2 at a system clock frequency of 200 MHz. Compared to the

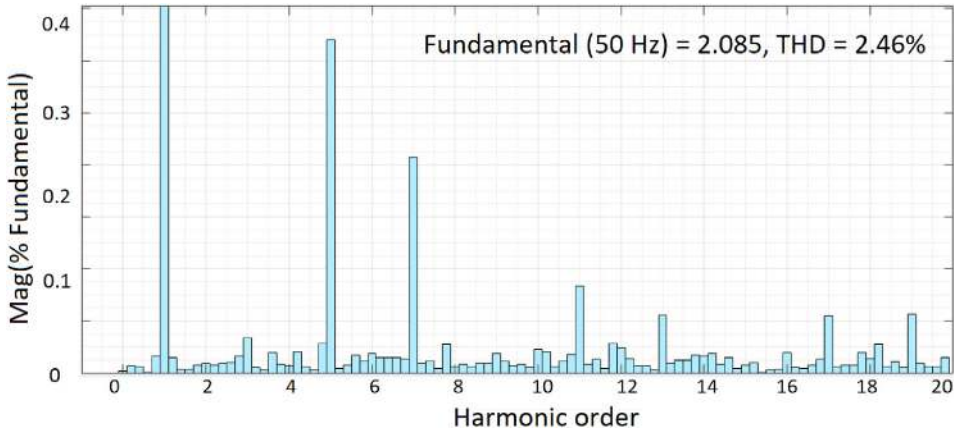


**FIGURE 9** THD plot of the load current for the proposed MPC

**TABLE 2** Computational requirements (200 MHz clock)

| Parameter | Conventional method | Proposed method |
|---|---|---|
| Clock cycles | 3258 | 2557 |
| Computational time | 15.8 μs | 12.7 μs |

weight factor-based method, the proposed predictive control does not require the calculation of supply-side inductor current and load inductor current in all the active vector cases are not necessary.

For a 200 MHz processor, the sampling time is 5 ns. From the code composer studio platform, it is observed that there are 3158 cycles required for the conventional MPC. So the operating time for the traditional predictive control is 15.79 seconds. In contrast, with the proposed predictive rule, it is 12.7 μs, which shows the computational requirements are $\approx 81\%$ of the total computations required by the weight factor-based method, which can be observed from 2. It offers a significant improvement while considering other calculations related to PLL, MPPT (for PV applications), and other auxiliary requirements such as ADC calculations. Comparison is performed under an identical sampling rate (ISR frequency) and the clock frequency of 200 MHz, which are reasonable for practical applications with grid-connected converters.

To conduct experimental studies, the prototype has been developed in the laboratory as shown in the Figure 10. AC side filter parameters are $L_1 = 1$ mH, $c_1 = 470\,\mu$F and the load filter value is $L_f = 10$ mH. The power rating of the developed qZS inverter configuration is 1.5 kW. The switching frequency considered of both methods is 8 kHz.

## 5.3 | Transient state and steady-state results

Figures 11 and 12 show the DC side steady-state measurements for the conventional MPC and proposed method, respectively, under the same operating conditions. It can be observed that both the methods reached steady-state reference values. However, the steady-state error is different for both approaches. In Figure 11, the steady-state ripple for the DC link voltage $(V_{\text{link}})$ is found to be 12 V, whereas the ripple with the proposed method (as shown in Figure 12) is only 4 V. The difference is due to the inductor current ripple variation. Inductor charging and discharging operations with the corresponding DC link voltage can also be observed from Figures 11 and 12. While comparing the inductor currents for both conventional MPC and the proposed method, the steady-state ripple is observed to be 1 A less with the proposed method (0.6 A) under the same operating conditions. The DC link voltage $(V_{\text{link}})$ shown is the sum of supply voltage and capacitor voltage.

The AC side steady-state results are shown in Figures 13 and 14 for the conventional MPC and proposed MPC, respectively. One of the main advantages of the proposed controller is the application of a double vector in a switching duration. From Figures 15 and 16, it can be observed from the steady-state results for a reference link voltage of 120 V that the proposed method produces a load current ripple of 0.25 A whereas the conventional method produces a load

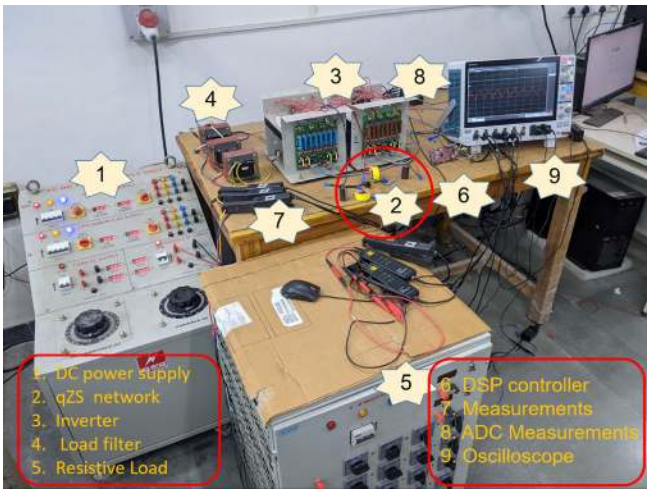


**FIGURE 10** Experimental setup used for implementing the proposed and conventional MPC algorithms

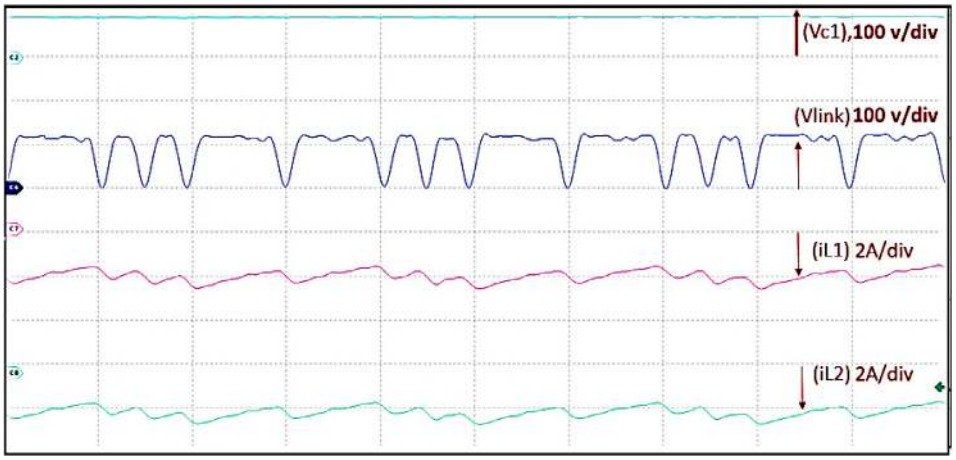


**FIGURE 11** DC side steady-state measurements for the conventional MPC

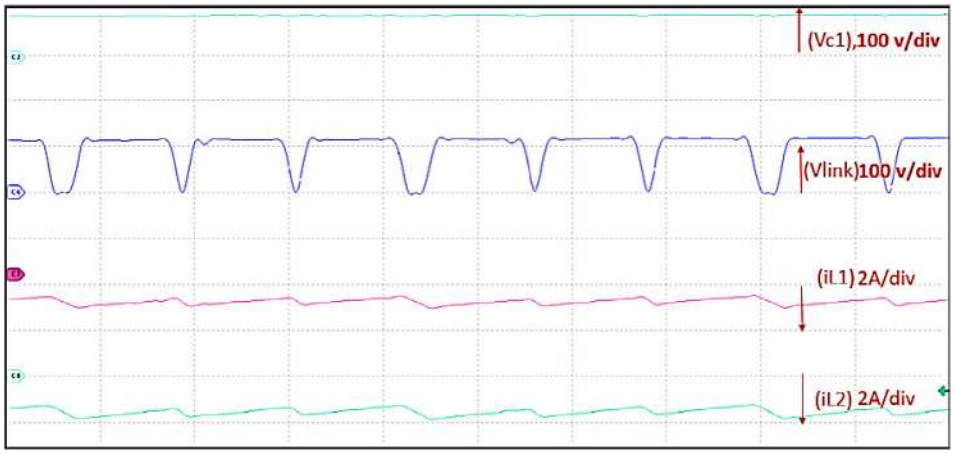


**FIGURE 12** DC side steady-state measurements for the proposed MPC

current ripple of 0.5 A. Figures 15 and 16 shows that the charging and discharging can be observed concerning voltage variation from 0 to 120 V or −120 to 0 V. This ripple variation is less in the proposed method due to the application of two vectors in a sampling period. This ripple reduction is achieved at a reference load current of 2 A. For both the

methods, load phase voltage is shown for A-phase. The presence of a higher ripple for the conventional MPC is due to the application of only a single vector in a sampling duration, as discussed in Section 4.2. When the link voltage reference is 160 V, the proposed method and the conventional method settle at the same steady-state value of 2.2 A whereas the ripple in case of the conventional method is 40% higher as compared to the proposed method which can be observed from Figures 17 and 18.

Figures 19 and 20 show the results for a step-change in the load power for conventional MPC and proposed MPC, respectively. Fast settling operation can be observed from both the figures, an inherent function of the basic OSV-MPC.

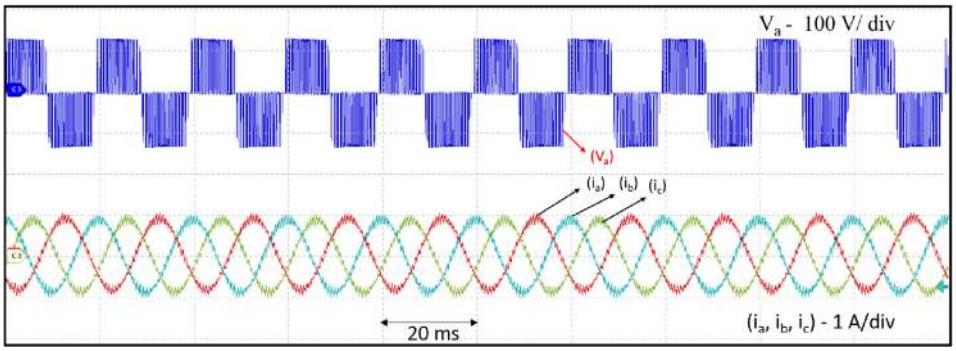


**FIGURE 13** AC side steady-state results with the conventional MPC at an AC frequency of $f_s = 50$ Hz and the DC link voltage reference of 120 V

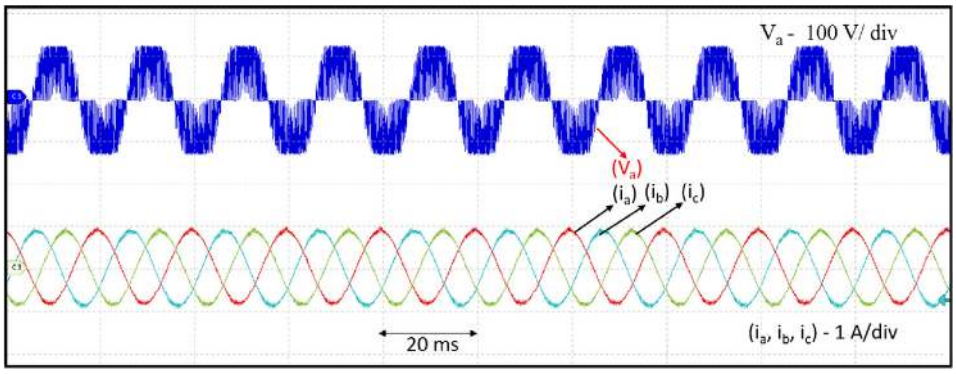


**FIGURE 14** AC side steady-state results with the proposed MPC at an AC frequency of $f_s = 50$ Hz and the DC link voltage reference of 120 V

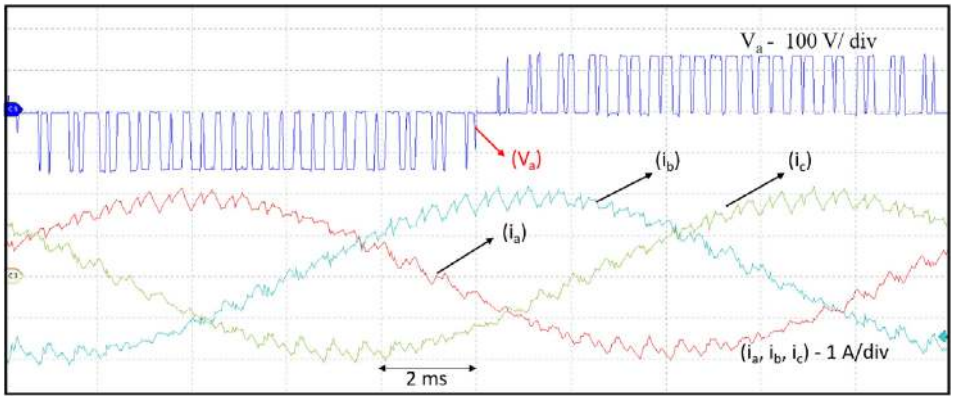


**FIGURE 15** Zoomed view of AC side steady-state results with the conventional MPC at an AC frequency of $f_s = 50$ Hz and the DC link voltage reference of 120 V

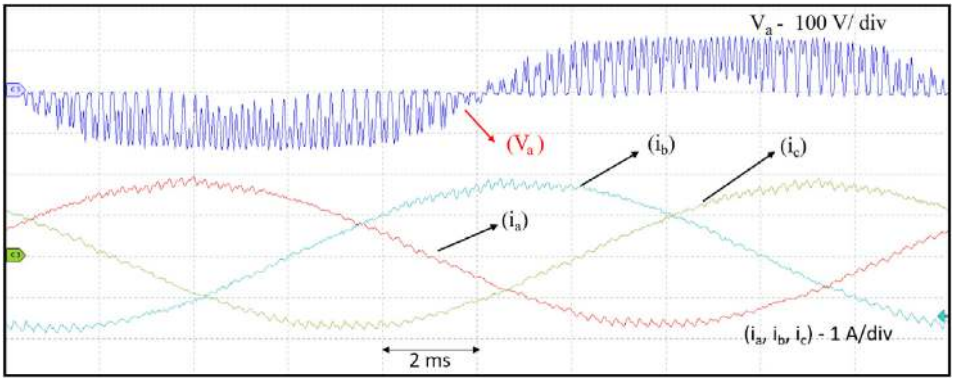


**FIGURE 16** Zoomed view of AC side steady-state results with the proposed MPC at an AC frequency of $f_s = 50$ Hz and the DC link voltage reference of 120 V

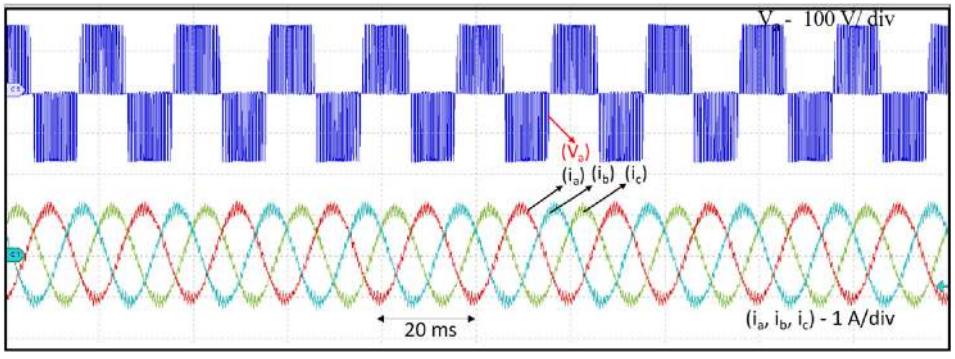


**FIGURE 17** AC side steady-state results with the conventional MPC at an AC frequency of $f_s$ =50 Hz and the DC link voltage reference of 160 V

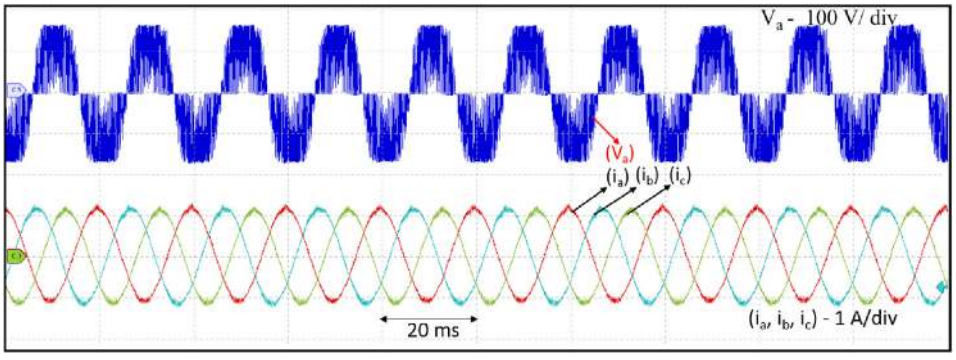


**FIGURE 18** AC side steady-state results with the proposed MPC at an AC frequency of $f_s$ =50 Hz and the DC link voltage reference of 160 V

Another observation from the inductor current is that the switching frequency (8 kHz) is high compared to the supply line frequency, common in MPC methods. The per-phase load current shown in both figures is stepped from 1 A RMS to 0.5 A RMS. The step-change in load current did not influence the steady-state value of the capacitor and the DC link voltage. However, the inductor has changed from 2.3 to 0.8 A in the conventional method and proposed method. It can also be observed that the ripple reduction affects the power losses in the system and parameter sensitivity as the real-time inductors inductance value gets changed with the current flowing through the inductor as well as the heat developed. The capacitor voltage (reference of 70 V) has not deviated from the step change in the load current for both methods.

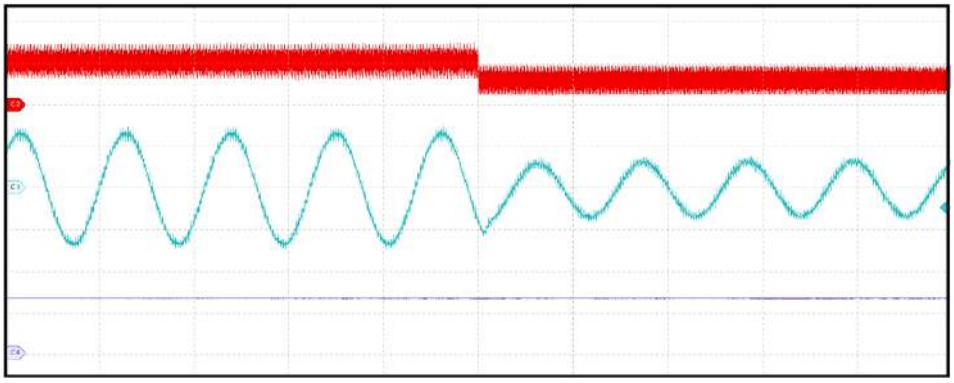

FIGURE 19 Results of the conventional MPC for the step change in the load power

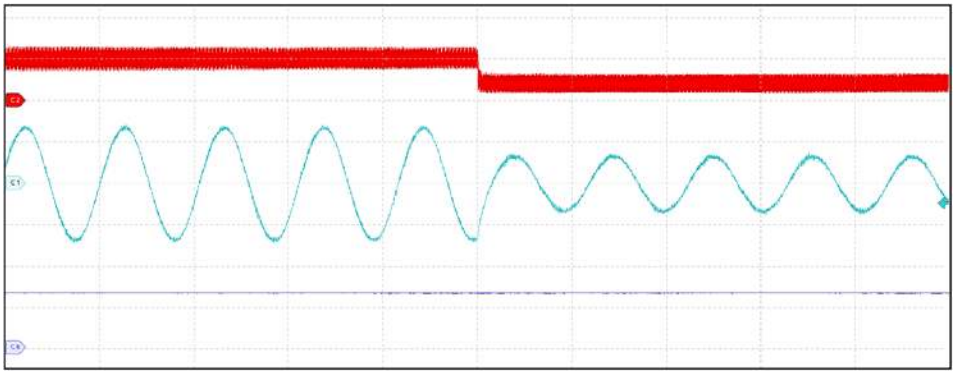

FIGURE 20 Results of the proposed MPC for the step change in the load power

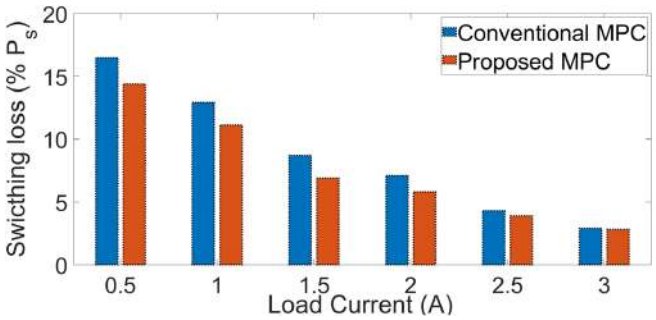


FIGURE 21 Switching loss comparison for the conventional and proposed methods with load variation

The equation for calculation of the switching losses can be expressed as,

$$p_{sw} = k\Delta i_c \Delta v_{ce} \tag{31}$$

where $k$ represents the proportional constant. $\Delta i_c$ represents the collector current and is the $\Delta v_{ce}$ collector-emitter voltage of the IGBT. Figure 21 shows the switching power loss against the load current variation. At low load currents, the percent value of switching losses is more but is obvious as the rated power is less. Higher the load current, lesser the switching loss variation in case of conventional method with respect to the proposed method. Equation to calculate the power loss per IGBT is.[47]

$$p_{\text{loss}} = p_{\text{loss,cond,ST}} + p_{\text{loss,cond,nST}} + p_{sw} \tag{32}$$

where $p_{\text{loss,cond,ST}}$ is the shoot-through conduction loss and $p_{\text{loss,cond,nST}}$ is the non-shoot-through conduction loss. $p_{sw}$ represents the switching losses of IGBT. The overall efficiency shown in Figure 22 has been calculated by considering the following equation.

$$\eta = \frac{P_{\text{out}}}{P_{\text{in}}} \tag{33}$$

where, the input power is obtained as, $P_{\text{in}} = V_{\text{DC}} I_L$ and the output power is obtained by using, $P_{\text{out}} = 3 v_a i_a \cos(\phi)$. Where, $I_L$ represents the inductor current, $V_{\text{DC}}$ represents the input DC voltage, $v_a$ represents the load phase voltage, $i_a$ represents the output phase current, and $\phi$ represents the phase angle between load voltage and load current. Figure 23 presents the load current THD variation with respect to the switching frequency. The value of load current error under steady-state is taken from the experimental wave forms. The percentage load current error $(i_{a,\text{error}}(\%))$ is calculated from the following equation.

$$(i_{a,\text{error}}(\%)) = \frac{i_{a,\text{act}} - i_{a,\text{ref}}}{i_{\text{ref}}} * 100 \tag{34}$$

where $i_{a,\text{act}}$ is the actual load current error and $i_{a,\text{ref}}$ is the reference load current. Proposed method is superior for all the modulation indices and also the load current tracking error is as low as 5% or less when the modulation index is above 0.8. Figure 24 presents the load current THD variation with respect to the switching frequency. The value of % load current THD is calculated from the FFT analysis. The formula used to obtain the same is given as,

$$(i_{a,\text{THD}}(\%)) = \frac{\sqrt{i_{a,\text{RMS}}^2 - i_{a,\text{fund}}^2}}{i_{a,\text{RMS}}} * 100 \tag{35}$$

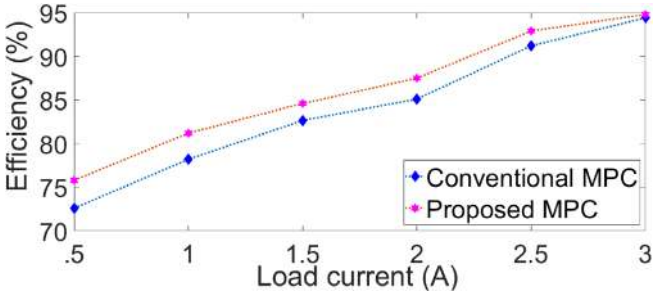


FIGURE 22 Efficiency comparison for the conventional and proposed methods with variation of load

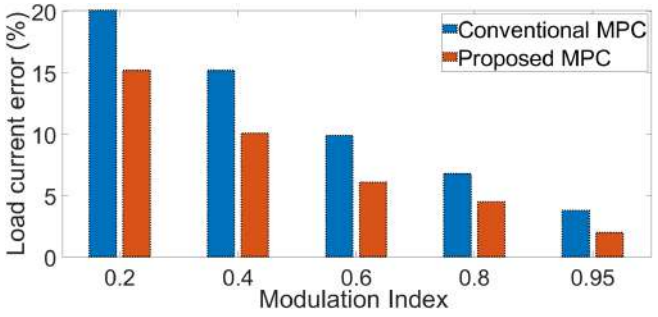


FIGURE 23 Load current tracking error performance with modulation index variation

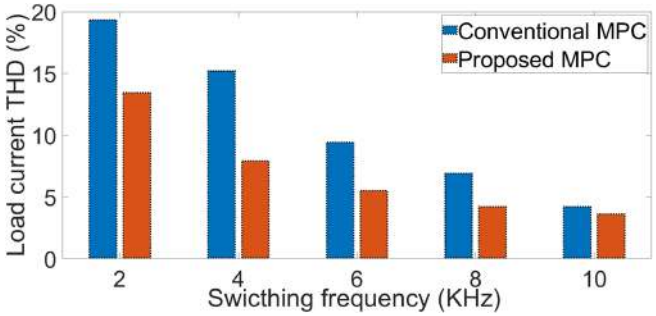


FIGURE 24 Load current THD performance with switching frequency variation

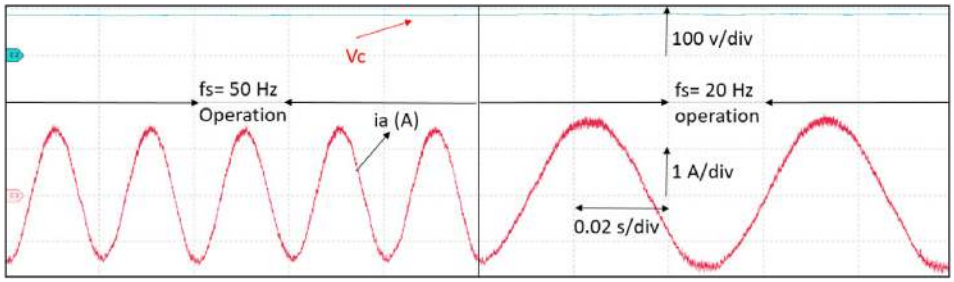


FIGURE 25 Load current reference frequency ($f_s$) step variation from 50 to 20 Hz with the proposed method


FIGURE 26 Results with phase unbalance in the reference and step change in the load with the proposed method at an AC frequency $f_s = 50$ Hz

Proposed MPC produces improved load current THD compared to the conventional MPC for all the switching frequencies.

## 5.4 | Special cases

Figure 25 has been presented as the special case where the load is balanced, but the reference current is changed from balanced to unbalanced at $t = 1$ second. The Load reference current for all the phases is 1 A before the reference change, and it is 1.5 A for one of the phases and 1 A for other phases after the change. An unbalanced load current reference has been considered at the step change, so the load current before and after the step follows the load current reference. The load current frequency change has been shown in Figure 26. Here the load current reference frequency has been changed from 50 to 20 Hz. It should be observed that the capacitor has not changed even after the frequency step change. This operation describes the control of capacitor voltage for changes in load frequency operation.

Buck mode operation of the qZSI with the proposed controller can be seen from Figure 27. For the supply voltage of 32.5 V, the capacitor voltage is nearly the same value as the supply voltage. The same can be observed from the DC link voltage, which is the same as the supply voltage for the buck mode of operation. Basically, for the buck mode of operation, the load current operation is only present with single variable control, as the shoot-through duty ratio is zero. However, the capacitor can be considered as a separate port, but that operation is application-specific. As the proposed method has the duty ratio at the DC and AC side, the inductor current ($i_{L_1}$) ripple and its frequency depend on the

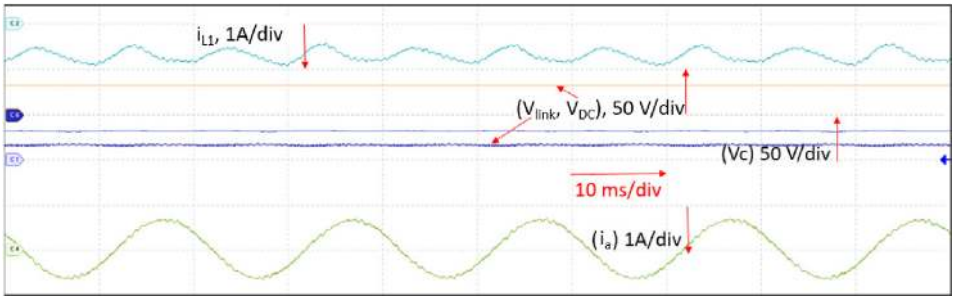


FIGURE 27 Results under Buck Mode of operation for the proposed method

TABLE 3 Comparison with previous MPC methods

| | Previous MPC methods | | | |
|---|---|---|---|---|
| | **Method in Mosa et al[33]** | **Method in Bakeer et al[40]** | **Method in Xu et al[41]** | **Proposed method** |
| Weight factors required | Yes | Yes | No | No |
| Switching frequency | Variable | Variable | Variable | Fixed |
| Inclusion of multi variables | Intuitive | intuitive | based on logic | intuitive |
| AC side multi vector operation | No | No | No | Yes |
| Modulation stage | Not available | Not available | Not available | Available |
| Computations with multi variables | High | Medium | based on logic | Low |
| Switching frequency reduction | Cumbersome | Cumbersome | based on logic | Flexible |
| Sampling frequency | High | Low | Low | Low |

inductance value and the operating modulation index similar to the conventional modulation techniques available for the qZSI.[48]

## 5.5 | Methodological comparison

Table 3 compares the advantages of the proposed MPC over the conventional MPCs available in the literature. The weight factor elimination method based on logical operations[41] is not a fixed frequency method, and it makes the filter design complex at the DC side and the AC side. In addition, the judgment logic has to be modified to include multiple control variables such as Common Mode voltage or thermal performance improvements. However, this is not the case with the proposed method, as the number of optimal vectors gets increased with the inclusion of additional control variables to get superior performance. Whereas with the other techniques such as,[33,40] the control of multiple variables is an intuitive approach. However, the intuitiveness gives superior performance under all the operating conditions only if the weight factor tuning is appropriate because the trial and error method requires the verification of many operating conditions with several simulation studies. As discussed in the introduction, several other methods such as fuzzy logic, PSO, and Artificial intelligence-based methods are required to tune the weight factors. Again this loses the intuitiveness of the conventional MPC. From Table 3, it can also be observed that one of the main advantages of the proposed MPC is the application of multiple vectors at the AC side as the application of more vectors in the switching sample increases the performance. However, at the cost of computational burden or predefined switching patterns.

From Table 3, it can be observed that the proposed algorithm only posses modulation method among all the predictive control algorithms of qZSI. Conventional shoot-through modulation methods such as simple boost, maximum boost, and maximum constant boost techniques can be included in the proposed method. Uniqueness of the proposed method is its reduced computations to the multi variable systems. As the proposed method evaluates only limited number of vectors for the subsequent variables, the computational efficiency is largely improved. This is not possible with

the conventional MPCs available in the literature. Inclusion of switching frequency reduction using the cost function based evaluation is flexible with the proposed method whereas in case conventional method, this advantage comes with the higher number of computational requirements.

### 5.6 | Limitations of the proposed MPC

The system provides good performance under normal operating conditions. But the performance slightly deteriorates because of the parameter mismatch. As the name indicates that the model predictive controller needs the detailed model of the system to calculate future (one step ahead or multi step ahead) values of the control parameters.

The switching frequency of the proposed MPC may slightly increase, during switching from active to zero vector which increases the steady-state ripple.

## 6 | CONCLUSION

This paper presents a double-vector predictive control algorithm for a three-phase quasi-ZSI without weight factors. Step by step implementation of the proposed controller has been provided with a flowchart and suitable equation. Clear improvements in the proposed algorithm such as weight factor elimination, steady-state ripple reduction, computational efficiency and fixed-frequency operation were presented, and a comparison containing the improvements in the proposed algorithm with the conventional predictive control algorithms are also presented. Besides the advantages, most of the commercial DSP micro controllers with clock frequency above 90 MHz can be used as the controller, and the total computational time comes around 13 μs (at 200 MHz) so that other auxiliary tasks can easily be implemented in the real-time operation. The results of the proposed control algorithm promise satisfactory operation under both buck and boost modes of operation, and also the same algorithm can be extended to any number of control variables by using multiple cost functions. In addition, the proposed algorithm is suitable for implementing the multi vector-based approaches if there exists sufficient computational power.

### PEER REVIEW

The peer review history for this article is available at https://publons.com/publon/10.1002/2050-7038.13068.

### DATA AVAILABILITY STATEMENT

Data sharing is not applicable to this article as no new data were created or analyzed in this study.

### ORCID

*Ravikumar Bhimasingu* https://orcid.org/0000-0002-5217-2598

### REFERENCES

1. Wu T, Chang C, Lin L, Kuo C. Power loss comparison of single- and two-stage grid-connected photovoltaic systems. *IEEE Tran Energy Convers*. 2011;26(2):707-715.
2. Mirafzal B, Saghaleini M, Kaviani AK. An SVPWM-based switching pattern for stand-alone and grid-connected three-phase single-stage boost inverters. *IEEE Trans Power Electron*. 2011 April;26(4):1102-1111.
3. Peng FZ. Z-source inverters. *Wiley Encycloped Electr Electron Eng*; 1999:1-11.
4. Anderson J, Peng FZ. Four quasi-Z-source inverters. In: 2008 IEEE Power Electronics Specialists Conference IEEE; 2008:2743–2749.
5. Ellabban O, Abu-Rub H. Z-source inverter: topology improvements review. *IEEE Ind Electron Mag*. 2016;10(1):6-24.
6. Rajasegharan V, Premalatha L, Rengaraj R. Modelling and controlling of PV connected quasi Z-source cascaded multilevel inverter system: an HACSNN based control approach. *Electr Pow Syst Res*. 2018;162:10-22.
7. Panda AK, Pandey R. Performance evaluation of controlled QZSI fed five-phase induction motor under voltage sag and interruption. *Int Trans Electr Energy Syst*. 2020;30(1):e12166.
8. Bajestan MM, Madadi H, Shamsinejad MA. Control of a new stand-alone wind turbine-based variable speed permanent magnet synchronous generator using quasi-Z-source inverter. *Electr Pow Syst Res*. 2019;177:106010.
9. Belila A, Berkouk EM, Benbouzid M, Amirat Y, Tabbache B, Mamoune A. Control methodology and implementation of a Z-source inverter for a stand-alone photovoltaic-diesel generator-energy storage system microgrid. *Electr Pow Syst Res*. 2020;185:106385.

10. Yi F, Cai W. A quasi-Z-source integrated multiport power converter as switched reluctance motor drives for capacitance reduction and wide-speed-range operation. *IEEE Trans Power Electron*. 2016;31(11):7661-7676.
11. Battiston A, Miliani EH, Pierfederici S, Meibody-Tabar F. Efficiency improvement of a quasi-Z-source inverter-fed permanent-magnet synchronous machine-based electric vehicle. *IEEE Trans Transport Electrif*. 2016;2(1):14-23.
12. Khajesalehi J, Hamzeh M, Sheshyekani K, Afjei E. Modeling and control of quasi Z-source inverters for parallel operation of battery energy storage systems: application to microgrids. *Electr Pow Syst Res*. 2015;125:164-173.
13. Guo F, Fu L, Lin CH, Li C, Choi W, Wang J. Development of an 85-kW bidirectional quasi-Z-source inverter with DC-link feed-forward compensation for electric vehicle applications. *IEEE Trans Power Electron*. 2013;28(12):5477-5488.
14. Chaib I, Berkouk EM, Gaubert J-P, Kermadi M, Sabeur N, Mekhilef S. An improved discontinuous space vector modulation for z-source inverter with reduced power losses. *IEEE Journal of Emerging and Selected Topics in Power Electronics*. 2021;9(3):3479-3488. http://doi.org/10.1109/jestpe.2020.3002684
15. Masaoud A, Sabeur N, Mekhilef S. Extended maximum boost control scheme based on single-phase modulator for three-phase Z-source inverter. *IET Power Electron*. 2015;10:9.
16. Sabeur N, Mekhilef S, Masaoud A. A simplified time-domain modulation scheme-based maximum boost control for three-phase quasi-Z source inverters. *IEEE J Emerg Selected Top Power Electron*. 2018;6(2):760-769.
17. Yaramasu V, Wu B. *Model Predictive Control of Wind Energy Conversion Systems*. 1st ed. Wiley Online Library: John Wiley & Sons; 2016: 91-116. https://onlinelibrary.wiley.com/doi/10.1002/9781119082989.ch3
18. González-Torres I, Miranda H, Méndez-Barrios CF, Espinoza J, Cárdenas V. Long-length horizons dynamic matrix predictive control for a MMC inverter. *Electr Pow Syst Res*. 2019;168:137-145.
19. Sahli A, Krim F, Laib A, Talbi B. Model predictive control for single phase active power filter using modified packed U-cell (MPUC5) converter. *Electr Pow Syst Res*. 2020;180:106139.
20. Kouro S, Cortés P, Vargas R, Ammann U, Rodrguez J. Model predictive control—a simple and powerful method to control power converters. *IEEE Trans Ind Electron*. 2008;56(6):1826-1838.
21. Chaves M, Margato E, Silva JF, Pinto SF, Santana J. HVDC transmission systems: bipolar back-to-back diode clamped multilevel converter with fast optimum-predictive control and capacitor balancing strategy. *Electr Pow Syst Res*. 2011;81(7):1436-1445.
22. Vazquez S, Marquez A, Leon JI, Franquelo LG, Geyer T. FCS-MPC and observer design for a VSI with output LC filter and sinusoidal output currents. In: 2017 11th IEEE Int. Conf. On Compatibility, Power Electronics and Power Engineering (CPE-POWERENG) IEEE; 2017:677-682.
23. Yaramasu V, Rivera M, Narimani M, Wu B, Rodriguez J. High performance operation for a four-leg NPC inverter with two-sample-ahead predictive control strategy. *Electr Pow Syst Res*. 2015;123:31-39.
24. Zhang Y, Xie W, Li Z, Zhang Y. Model predictive direct power control of a PWM rectifier with duty cycle optimization. *IEEE Trans Power Electron*. 2013;28(11):5343-5351.
25. Wang B, Xian L, Manandhar U, et al. Hybrid energy storage system using bidirectional single-inductor multiple-port converter with model predictive control in DC microgrids. *Electr Pow Syst Res*. 2019;173:38-47.
26. Gannamraju SK, Valluri D, Bhimasingu R. Comparison of fixed switching frequency based optimal switching vector MPC algorithms applied to voltage source inverter for stand-alone applications. In: 2019 National Power Electronics Conference (NPEC) IEEE; 2019:1-6.
27. Tarisciotti L, Zanchetta P, Watson A, Bifaretti S, Clare JC. Modulated model predictive control for a seven-level cascaded H-bridge back-to-back converter. *IEEE Trans Ind Electron*. 2014;61(10):5375-5383.
28. Yang Y, Wen H, Li D. A fast and fixed switching frequency model predictive control with delay compensation for three-phase inverters. *IEEE Access*. 2017;5:17904-17913.
29. Chen J, Li Y. Virtual vectors based predictive control of torque and flux of induction motor and speed sensorless drives. In: Conference Record of the 1999 IEEE Industry Applications Conference. Thirty-Forth IAS Annual Meeting (Cat. No. 99CH36370), vol. 4 IEEE; 1999: 2606-2613.
30. Shi X, Zhu J, Li L, Lu DDC. Low-complexity dual-vector-based predictive control of three-phase PWM rectifiers without duty-cycle optimization. *IEEE Access*. 2020;8:77049-77059.
31. Zhang Y, Qu C. Model predictive direct power control of PWM rectifiers under unbalanced network conditions. *IEEE Trans Ind Electron*. 2015;62(7):4011-4022.
32. Ellabban O, Mosa M, Abu-Rub H, Rodríguez J. Model predictive control of a grid connected quasi-Z-source inverter. In: 2013 IEEE International Conference on Industrial Technology (ICIT); 2013:1591-1596.
33. Mosa M, Balog RS, Abu-Rub H. High-performance predictive control of quasi-impedance source inverter. *IEEE Trans Power Electron*. 2016;32(4):3251-3262.
34. Li Y, Jiang S, Cintron-Rivera JG, Peng FZ. Modeling and control of quasi-Z-source inverter for distributed generation applications. *IEEE Trans Ind Electron*. 2013;60(4):1532-1541.
35. Rojas CA, Rodriguez J, Villarroel F, Espinoza JR, Silva CA, Trincado M. Predictive torque and flux control without weighting factors. *IEEE Trans Ind Electron*. 2013;60(2):681-690.
36. Mahmoudi H, J Lesani M, Arab Khabouri D. Online fuzzy tuning of weighting factor in model predictive control of PMSM. In: 2013 13th Iranian Conference on Fuzzy Systems (IFSC); 2013:1-5.
37. Hassani AM, Bektas SI, Hosseini SH. Modular multilevel converter circulating current control using model predictive control combined with genetic algorithm. *Proc Comput Sci*. 2017;120:780-787.

38. Dragičević T, Novak M. Weighting factor design in model predictive control of power electronic converters: an artificial neural network approach. *IEEE Trans Ind Electron*. 2019;66(11):8870-8880.
39. Bakeer A, Ismeil MA, Orabi M. Grid connection quasi Z-source inverter based on model predictive control with less sensors count. 2016 Eighteenth International Middle East Power Systems Conference (MEPCON); 2016:591-596.
40. Bakeer A, Ismeil MA, Orabi M. A powerful finite control set-model predictive control algorithm for quasi Z-source inverter. *IEEE Trans Ind Inform*. 2016;12(4):1371-1379.
41. Xu Y, He Y, Li S. Logical operation based model predictive control for quasi Z-source inverter without weighting factor. IEEE Journal of Emerging and Selected Topics in Power Electronics; 2020.
42. Liu C, Liu P, Luo H, Huang S, Xu J. A new model predictive control strategy for quasi-Z-source inverters. In: 2019 22nd International Conference on Electrical Machines and Systems (ICEMS); 2019:1-5.
43. Qin S, Liu P, Huang S. A robust modified model predictive control algorithm for quasi-Z source inverters. In: 2019 22nd International Conference on Electrical Machines and Systems (ICEMS) IEEE; 2019:1-5.
44. Norambuena M, Rodriguez J, Zhang Z, Wang F, Garcia C, Kennel R. A very simple strategy for high-quality performance of ac machines using model predictive control. *IEEE Trans Power Electron*. 2018;34(1):794-800.
45. Zhang Y, Zhang B, Yang H, Norambuena M, Rodriauez J. Generalized sequential model predictive control of induction motor drives. In: 2018 21st International Conference on Electrical Machines and Systems (ICEMS) IEEE; 2018:1285-1290.
46. Cortés P, Kouro S, La Rocca B, et al. Guidelines for weighting factors adjustment in finite state model predictive control of power converters and drives. In: Proc. IEEE Int. Conf. Ind. Tech. (ICIT); 2009:1-7.
47. Grgić I, Vukadinović D, Bašić M, Bubalo M. Calculation of semiconductor power losses of a three-phase quasi-z-source inverter. *Electronics*. 2020;9(10):1-19. http://doi.org/10.3390/electronics9101642
48. Florez-Tapia AM, Ibanez FM, Vadillo J, Elosegui I, Echeverria JM. Small signal modeling and transient analysis of a trans quasi-Z-source inverter. *Electr Pow Syst Res*. 2017;144:52-62.


**How to cite this article:** Gannamraju SK, Bhimasingu R. Sequential model predictive control of quasi Z-source inverter with fixed frequency operation. *Int Trans Electr Energ Syst*. 2021;e13068. doi:10.1002/2050-7038.13068